Am J Nucl Med Mol Imaging 2016;6(1):42-58
www.ajnmmi.us /ISSN:2160-8407/ajnmmi0016443

Original Article

Biodistribution of the radionuclides ^{18}F-FDG, ^{11}C-methionine, ^{11}C-PK11195, and ^{68}Ga-citrate in domestic juvenile female pigs and morphological and molecular imaging of the tracers in hematogenously disseminated *Staphylococcus aureus* lesions

Pia Afzelius[1], Ole L Nielsen[2], Aage KO Alstrup[3], Dirk Bender[3], Páll S Leifsson[2], Svend B Jensen[4,5], Henrik C Schønheyder[6,7]

[1]Department of Diagnostic Imaging, North Zealand Hospital, Hillerød, Denmark; [2]Department of Veterinary Disease Biology, University of Copenhagen, Copenhagen, Denmark; [3]Department of Nuclear Medicine and PET Centre, Aarhus University Hospital, Aarhus, Denmark; [4]Department of Nuclear Medicine, Aalborg University, Aalborg, Denmark; [5]Department of Chemistry and Biochemistry, Aalborg University, Aalborg, Denmark; [6]Department of Clinical Microbiology, Aalborg University Hospital, Aalborg, Denmark; [7]Department of Clinical Medicine, Aalborg University, Aalborg, Denmark

Received September 19, 2015; Accepted October 29, 2015; Epub January 28, 2016; Published January 30, 2016

Abstract: Approximately 5-7% of acute-care patients suffer from bacteremia. Bacteremia may give rise to bacterial spread to different tissues. Conventional imaging procedures as X-ray, Computed Tomography (CT), Magnetic Resonance Imaging (MRI), and ultrasound are often first-line imaging methods for identification and localization of infection. These methods are, however, not always successful. Early identification and localization of infection is critical for the appropriate and timely selection of therapy. The aim of this study was thus; a head to head comparison of ^{18}F-fluorodeoxyglucose (^{18}F-FDG) positron emission tomography (PET) to PET with tracers that potentially could improve uncovering of infectious lesions in soft tissues. We chose ^{11}C-methionine, ^{11}C-PK11195, and ^{68}Ga-citrate as tracers and besides presenting their bio-distribution we validated their diagnostic utility in pigs with experimental bacterial infection. Four juvenile 14-15 weeks old female domestic pigs were scanned seven days after intra-arterial inoculation in the right femoral artery with a porcine strain of *S. aureus* using a sequential scanning protocol with ^{18}F-FDG, ^{11}C-methionine, ^{11}C-PK11195 and ^{68}Ga-citrate. This was followed by necropsy of the pigs consisting of gross pathology, histopathology and microbial examination.The pigs primarily developed lesions in lungs and neck muscles. ^{18}F-FDG had higher infection to background ratios and accumulated in most infectious foci caused by *S. aureus*, while ^{11}C-methionine and particularly ^{11}C-PK11195 and ^{68}Ga-citrate accumulated to a lesser extent in infectious foci. ^{18}F-FDG-uptake was seen in the areas of inflammatory cells and to a much lesser extent in reparative infiltration surrounding necrotic regions.

Keywords: Osteomyelitis, domestic pigs, porcine, swine, *Staphylococcus aureus*, positron emission tomography, computed tomography, infection, ^{18}F-FDG, ^{68}Ga-citrate, ^{11}C-methionine, ^{11}C-PK11195, animal

Introduction

Staphylococcus aureus infections are frequent and even increasing, and constitute a significant global healthcare burden [1, 2]. Diagnosis, management, and control of this infection are important issues, because failure to recognize patients with infection and lack of understanding of the pitfalls of empirical antimicrobial selection are associated with a high mortality rate in otherwise healthy people. In spite of advances in medical care and discovery of potent anti-staphylococcal antibiotics, about one fourth of patients with *S. aureus* bacteremia die within 30 days [3]. Since the emergence of methicillin-resistant *S. aureus* strains (MRSA) in the 1960s, resistance to additional classes of antibiotics have appeared continuously, leav-

ing few therapeutic options for some of the widespread clones [4]. Vancomycin remains a mainstay for treatment of MRSA although a resistant phenotype may be inducible; linezolid and Daptomycin are important alternative options [5]. Either the primary focus or secondary lesions formed by dissemination of *S. aureus* may maintain the infection in spite of otherwise correctly instituted treatment demanding anatomical identification and perhaps surgical intervention. Imaging of infections is challenging and no ideal imaging modality has yet been found. The ideal imaging modality and/or biomarker should distinguish infection from inflammation with high sensitivity and specificity, should e.g. not relate to the stage of infection, the anatomical localization or blood flow, and be both cost-effective and easily available.

Traditional nuclear infection imaging includes labeled leukocyte scintigraphy which has been used since the 1970s [6, 7]. *In vitro* labeling of leukocytes is time consuming, poses a personnel safety risk of radiation exposure, infection, and cross-contamination as it involves isolating leukocytes from a patient, labeling the leukocytes *in vitro*, and finally re-injecting the leukocytes.

Gallium is a metallic ion that is taken up by infectious and inflammatory sites [8] and ^{67}Ga-citrate scintigraphy was the leading modality for imaging of inflammation and infection of musculoskeletal origin in the 1970s and the early 1980s [9-13], but the often inadequate injectable activity (necessitated by the long half-life) and the wide spectrum of gammas emitted by ^{67}Ga reduce image quality and resolution. Other drawbacks are the high background activity, interference from liver and bowel activity, delayed post injection imaging of at least 48-72 h, the associated high radiation exposure, and high cost of the radionuclide.

^{18}F-flourodeoxyglucose (FDG) is a multipurpose PET tracer with high sensitivity, but has the limitation that a highly metabolically active lesion may indicate presence of not only infection but also inflammatory, reparative, or reactive changes as well as cancer [14]. Another limitation would be the incorrect interpretation in those organs and tissues with high normal FDG-metabolic activity or -excretion, overlooking an infectious, a cancerous, or an inflammatory focus.

We have previously reported the ability of various radionuclides to visualize *S. aureus* osteomyelitis in pigs [15] inoculating the femoral artery of the right hind limb to produce osteomyelitis foci here [15, 16]. Accidentally, *S. aureus* did not settle in the bones exclusively, but clear signs of systemic spread were recognized by documentation of *S. aureus* in e.g. lung tissue. In the present study, we report the results of PET/CTs of lung abscesses and infectious lesions located elsewhere related to the model-infection in those pigs. We aimed both to characterize the bio-distribution of tracers in juvenile female pigs and to compare the utility of ^{18}F-FDG, ^{11}C-methionine, ^{11}C-PK11195 ([N-Methyl-^{11}C](R)-1-(2-chlorophenyl)-N-(1-methylpropyl)-3-isoquinoline carboxamide), and ^{68}Ga-citrate.

Methionine is a naturally occurring essential amino acid and it can be labeled with the positron-emitting isotope ^{11}C. Methionine, which is transported into cells via the L-type amino acid transporter 1, is crucial for the formation of proteins and is involved in the synthesis of phospholipids. Methionine thus reflects amino acid transport and protein synthesis and when cells replicate the demand for proteins, phospholipid synthesis, and essential amino acids increases. Although L-[methyl-^{11}C] methionine (^{11}C-methionine) is known to accumulate in inflammatory lesions [17], it is primarily used for detection of brain tumors [18].

^{11}C-PK11195 is an isoquinoline carboxamide and a high-affinity ligand for the 18 kDa mitochondrial translocator protein (TSPO), previously known as the peripheral benzodiazepine receptor (PBR). TSPO is highly expressed on activated mononuclear phagocytic cells and ^{11}C-PK11195 has typically been used to diagnose neuroinflammation [19, 20]. It has also been used in an attempt to visualize inflammation at other anatomical sites, e.g. in macrophage-dominated infiltrates of blood vessels and tissue membranes surrounding loosening prostheses in rat models [21, 22] and in humans [23]. Despite the widespread use of ^{11}C-PK11195 PET, the whole-body distribution and dosimetry of ^{11}C-PK11195 have not been studied until recently [24-26].

^{68}Ga-citrate is a marker of infection and has been demonstrated to accumulate solely in infectious lesions [27], but compared to ^{67}Ga,

^{68}Ga has a shorter half-life, is effective within 60 min post-injection imaging time, is cost-effective, will cause less radiation exposure, and will cause less background liver and bowel activity. The cellular uptake of ^{68}Ga-citrate is not fully understood, but ^{68}Ga-citrate binds to lactoferrin present in high concentrations in neutrophils, abscess fluid and in the bacterial siderophores [28-30].

We hypothesize that some of the less well studied radionuclides in the context of infection can detect infectious lesions in lung and connective tissues derived from hematogenously spread of *S. aureus* in pigs.

Material and methods

Pigs and the osteomyelitis model

We have previously reported the design of the study, the clinical signs, hematology, pathology and scans related to infection of the hind limbs and pelvic region [15]. The materials and methods section here thus only briefly state the various protocols.

Four clinically healthy, female, specific pathogen-free (SPF), Danish landrace cross-breed pigs, aged 13-14 weeks were under anesthesia inoculated with a porcine strain of *S. aureus* into the femoral artery of the right hind limb using the technique described by Johansen and Jensen et al. [16]. One week later the pigs were anesthetized and scanned, followed by euthanasia and necropsy.

The study was approved by the Danish Animal Experimentation Board, journal no. 2012-15-2934-000123. All facilities were approved by the Danish Occupational Health Surveillance.

Microbiology

The inoculum was prepared from the S54F9 strain of *S. aureus* (spa type t1333, MLST sequence type ST433 and clonal complex CC30), isolated from a chronic embolic pulmonary abscess in a pig [31-33]. Overnight grown cultures on 5% horse blood agar (HBA) (SSI Diagnostica, Denmark) were harvested and suspended in 0.9% sterile saline. Inocula ranged from 10.5×10^3 to 141×10^3 colony forming units per kg bodyweight suspended in 1.0 to 3.5 ml of sterile saline.

Tissue specimens and swabs obtained at necropsy were plated on 5% HBA and read after incubation overnight. *S. aureus* was confirmed by colony morphology and latex agglutination (Monostaph Plus, Bionor Laboratories, Norway). Growth characteristics including a pansusceptible antibiogram were taken to indicate identity with the inoculated strain. Contaminants were sparse and characterized primarily by Gram stain. A few isolates were identified to species level by matrix-assisted laser desorption/ionization-time of flight (MALDI-TOF) (Bruker Daltonik GmbH, Bremen, Germany).

Preparation of tracers

^{11}C and ^{18}F were produced at the PET Center Aarhus using either a PETtrace 800 series cyclotron (GE Healthcare, Uppsala, Sweden) or a Cyclone 18/18 cyclotrone (IBA, Louvain La Neuve, Belgium). ^{68}Ga was obtained at the department of Nuclear Medicine in Aalborg by eluting a ^{68}Ge/^{68}Ga generator (IGG100; Eckert & Ziegler AG Eurotope GmbH).

^{18}F-FDG was produced by a standard procedure applying a GE Healthcare MX Tracerlab synthesizer, Mx cassettes supplied by Rotem Industries (Arava, Israel) and chemical kits supplied by ABX GmbH (Radeberg, Germany). The radiochemical purity was higher than 99%.

^{11}C-methionine was synthesized by [^{11}C] *S*-methylation of L-homocystein thiolactone with methyl iodide [34] followed by semipreparative HPLC using a GE Healthcare Tracerlab FXC PRO synthesizer. L-Homocysteine thiolactone was supplied by Sigma (Sigma-Aldrich Denmark, Brøndby, Denmark). Other chemicals including iodine or acetone were supplied by either Aldrich (Sigma-Aldrich Denmark, Brøndby, Denmark) or Aarhus University Hospital Pharmacy (Aarhus, Denmark). The radiochemical purity exceeded 95% and the specific radioactivity generally was higher than 37 GBq/μmol.

^{11}C-PK11195 was prepared by *N*-methylation of desmethyl-PK11195 with methyl iodide [35] followed by semipreparative HPLC and solid phase extraction using a GE Healthcare Tracerlab FXC PRO synthesizer. Desmethyl-PK11195 was supplied by ABX GmbH (Radeberg, Germany). All other chemicals were supplied by either Aldrich (Sigma-Aldrich Denmark,

Brøndby, Denmark) or Aarhus University Hospital Pharmacy (Aarhus, Denmark). The radiochemical purity exceeded 95% and the specific radioactivity generally was higher than 50 GBq/μmol.

^{68}Ga-citrate was synthesized in high yield within 10 min and without the use of organic solvents as described earlier [36]. Briefly, the synthesis was conducted using a fully automated cassette-based system (Modular-Lab PharmTracer) as well as cassettes from Eckert & Ziegler Eurotope GmbH. The ultrapure hydrochloric acid (30%) was obtained from Merck. Other chemicals were from either Aldrich (Sigma-Aldrich Denmark) or Aalborg University Hospital Pharmacy (Aalborg, Denmark). The tracer had purity close to 100% and had a very low content of Germanium-68.

CT and PET

At the day of the scan, the pigs (body weight 39-42 kg) were handled as described earlier [15, 37]. All examinations at the PET Center Aarhus were performed with an integrated PET/CT system (Siemens Biograph True point 64 PET/CT, Siemens, Erlangen, Germany). The pigs were placed in recumbency. Initially a scout view was obtained to secure body coverage from snout to tail. Attenuation correction of CT data was obtained first, based on low dose CT maps. CT and PET data were co-registered, and image fusion was performed using the iterative TrueX algorithm (Siemens).

At the Nuclear Medicine Department in Aalborg pigs were placed in recumbent position and whole-body PET/CTs were performed with an integrated system (GE VCT discovery True 64 PET/CT 2006, GE Healthcare, USA) essentially as in Aarhus. PET images were reconstructed using a fully 3-dimensional iterative algorithm (ViewPoint algorithm (GE Healthcare)), and attenuation correction was based on low-dose CT.

The sequence of tracer injections (scans) was ^{11}C-Methionine, ^{11}C-PK11195, ^{68}Ga-citrate, and ^{18}F-FDG. PET was performed 1 h 5 min after injection of 408-500 MBq of ^{11}C-Methionine, 1 h 5 min after injection of 263-464 MBq ^{11}C-PK11195, 1 h - 1 h 13 min after injection of 113-175 MBq of ^{68}Ga-citrate, and 1 h - 1 h 34 min after injection of 299-389 MBq of ^{18}F-FDG.

The minimum timespan from first injection to last scan was 13 h 9 min (pig 4); the maximum timespan was 14 h 45 min (pig 1).

Reading the scans

Computed tomography with ^{18}F-FDG, ^{11}C-Methionine, ^{11}C-PK11195 and ^{68}Ga-citrate PET were read individually and also as fused images with CT. All scans were evaluated by both a nuclear physician and a veterinarian.

Gross pathology and histopathology

Necropsy was performed according to Madsen and Jensen [38], and as reported previously [15] and predefined tissues and organs were sampled for microbial cultivation and histopathology. Thus, biopsies or swabs for microbial cultivation were obtained from the lungs, brain, liver, spleen, and kidney, and histopathology was performed on lung and abscesses.

Identification of gross lesions at necropsy generally resulted in additional sampling for microbiology and histopathology. Additional sampling for microbiology included pleura fluid from pigs 2 and 4, a muscle lesion from pig 3, and abdominal cavity fluid from all four pigs. Additional histopathology included necrotic muscle foci from pigs 1, 2 and 3, and trachea from pig 4. For histopathology, samples were fixated in 3.7% neutral buffered formaldehyde for 4 days, kept in 70% ethanol for 3-5 weeks, dehydrated and embedded in paraffin wax, cut in 3 μm thick sections, mounted on glass slides, stained with hematoxylin and eosin, and cover slipped according to standard procedures. An immunohistochemical protocol for the detection of *S. aureus* (in a muscle lesion form pig 1) was performed as described [39] using a monoclonal mouse antibody to *S. aureus*.

Results

Bio-distribution

The physiological (background) uptake and readability of the different radionuclides were recorded and bio-distribution of PET tracers in juvenile female pigs, which was readily recog-

Table 1. Bio-distribution of ^{18}F-FDG in juvenile 14-15 weeks old female domestic pigs. List of target tissues/organs encompassed by region of interest. Median values of SUV_{min}, SUV_{max}, and SUV_{mean}. Ranges in parentheses

^{18}F-FDG	SUV_{min}	SUV_{max}	SUV_{mean}
Brain	2.8 (1.9-3.0)	3.65 (3.1-5.1)	3.15 (2.4-3.9)
Thymus	0.95 (0.6-1.3)	2.4 (2.17-2.6)	1.75 (1.4-2.6)
Heart	0.55 (0.2-1.5)	0.95 (0.6-8.8)	0.55 (0.5-1.2)
Lung	0.4 (0.2-0.7)	0.6 (0.3-1.0)	0.5 (0.3-0.9)
Vertebral body	0.8 (0.1-0.8)	1.35 (0.7-1.5)	1.1 (0.5-1.3)
Liver	1.0 (0.9-1.2)	1.4 (1.3-1.7)	1.15 (1.1-1.4)
Spleen	0.85 (0.6-1.0)	1.6 (1.2-2.4)	1.3 (0.9-1.6)
Gall bladder	0.8	1.2	0.9
Stomach	0.1 (0.1-0.1)	0.3 (0.2-0.6)	0.15 (0.1-0.2)
Small intestine	2.0 (1.8-2.3)	2.75 (2.4-4.0)	2.4 (2.1-3.0)
Colon	0.75 (0.5-0.8)	2.0 (3.3-6.0)	1.3 (0.9-1.5)
Kidney	1.3 (0.9-1.2)	1.4 (1.3-1.7)	1.15 (1.1-1.4)
Urine bladder	4.6 (0.9-10.7)	40.4 (11.7-58.2)	19.5 (9.8-26.6)
Tight muscle	0.1 (0.1-0.1)	0.2 (0.2-0.5)	0.3 (0.1-0.0.2)
Swallowing muscles	1.45 (0.9-2.0)	7.5 (5.0-11)	4.1 (4.0-4.9)
Sinus	2.55 (2.1-3.3)	7.55 (5.3-10.7)	5.05 (4.5-7.6)

Table 2. Bio-distribution of ^{11}C-Methionone in juvenile 14-15 weeks old female domestic pig. List of target tissues/organs encompassed by region of interest. Median values of SUV_{min}, SUV_{max}, and SUV_{mean}. Ranges in parentheses

^{11}C-Methionine	SUV_{min}	SUV_{max}	SUV_{median}
Brain	0.1 (0.1-0.2)	3.2 (2.7 -4.9)	1.0 (0.9-1.0)
Thymus	0.15 (0.1-0.2)	8.3 (7.2-8.8)	2.15 (1.8-2.2)
Heart	0.1 (0.1-0.1)	4.25 (3.9-5.2)	1.0 (0.7-1.3)
Lung	0.0 (0.0-0.1)	3.2 (2.3-3.6)	0.7 (0.5-0.8)
Vertebral body	0.3 (0.2-0.4)	7.85 (8.9-10.7)	2.5 (2.1-2.9)
Liver	0.85 (0.3-0.7)	9.05 (6.7)	2.9 (1.7-4.2)
Spleen	0.2 (0.1-0.2)	3.85 (3.3-4.3)	1.35 (1.0-1.5)
Gall bladder	0.1 (0.1-0.1)	3.45 (3.0-3.6)	0.7 (0.6-0.8)
Stomach	0.0 (0.0-0.1)	3.25 (1.0-4.7)	0.35 (0.2-1.0)
Pyloric antrum/duodenum	0.65 (0.4-0.9)	6.8 (5.8-8.2)	2.6 (1.9-3.4)
Small intestine	0.9 (0.5-1.9)	10.75 (9.7-14.7)	5.5 (3.8-7.2)
Colon	0.1 (0.0-0.6)	4.95 (3.3-6.0)	1.05 (1.0-1.6)
Kidney	0.9 (0.3-1.0)	8.85 (6.8-9.7)	3.65 (2.8-3.7)
Urine bladder	-	-	-
Tight muscle	0.1 (0.1-0.1)	3.2 (2.3-3.6)	0.6 (0.0.5-0.8)

nizable as areas of prominent activity on emission images, is presented in **Tables 1**-**4**. Some organs such as salivary glands and pancreas could not be quantified because of the imprecision of localization on *non*-contrast, low-resolution CT scans in small sized pigs. Whole body activity of different tracers is presented in **Figure 1**.

Very high ^{18}F-FDG activity was seen in the urine bladder and in the ethmoturbinates (**Figure 1**) and less activity was seen in the sinuses of the head, pharyngeal tissue, small intestine, and thymus (**Table 1**). Variable activity was seen in the left ventricle of the heart, low activity was seen in brain and liver and slight activity was seen in muscle tissue, stomach, and lungs.

The highest concentrations of ^{11}C-methionine were found in small intestine (**Figure 1**), liver, kidney, thymus, pyloric antrum/duodenum, and bones (**Table 2**), less activity was seen in other regions, such as the colon, heart and brain andslight activity was seen in the urine bladder.

High radioactivity after venous injection of ^{11}C-PK11195 was found in the gall bladder (**Figure 1**), pyloric antrum/duodenum, urine bladder, and small intestine (**Table 3**), less activity was seen in other regions, such as bone, liver, kidney, and thymus and slight activity was seen in the lungs and muscle tissues.

High activity of ^{68}Ga-citrate was seen in the small intestine and in bone (**Figure 1**), especially in the growth zones (**Table 4**) and almost no activity was seen in muscle tissue, the brain, and gall bladder.

CT, gross pathology, microbiology and histopathology

Here we report findings related to the head, neck, thorax, and abdomen (**Table 5**) and of significance to the present study and as earlier

Table 3. Bio-distribution of ^{11}C-PK11195 in juvenile 14-15 weeks old female domestic pigs. List of target tissues/organs encompassed by region of interest. Median values of SUV_{min}, SUV_{max}, and SUV_{mean}. Ranges in parentheses

^{11}C-PK11195	SUV_{min}	SUV_{max}	SUV_{mean}
Brain	0.1 (0.1-0.1)	2.3 (2.0 -2.9)	0.6 (0.5-0.8)
Thymus	0.6 (0.1-1.1)	5.2 (4.7-6.2)	1.9 (1.12-2.3)
Heart	0.05 (0.0-0.1)	5.05 (4.2-6.2)	0.85 (0.8-1.0)
Lung	0.05 (0.0-0.1)	1.9 (1.9-2.0)	0.5 (0.4-0.6)
Vertebral body	0.45 (0.3-0.6)	8.5 (8.3-11.0)	3.05 (2.4-3.2)
Liver	0.45 (0.3-0.7)	7.75 (5.8-8.6)	2.2 (1.9-2.6)
Spleen	0.15 (0.1-0.2)	3.85 (3.4-4.7)	1.1 (0.9-1.1)
Gall bladder	1.2 (0.1-4.4)	25.5 (1.2-37.8)	11.35 (0.4-16.4)
Stomach	0.0 (0.0-0.1)	3.5 (1.0-3.9)	0.4 (0.1-1.0)
Pyloric antrum/duodenum	1.55 (1.0-3.8)	20.1 (12.61-41.1)	9.65 (4.1-15.2)
Small intestine	1.0 (0.5-1.9)	9.25 (8.6-9.4)	3.55 (2.6-4.6)
Colon	0.05 (0.0-0.3)	4.8 (4.3-5.4)	1.0 (0.8-1.9)
Kidney	0.25 (0.2-0.4)	6.2 (4.8-6.6)	1.8 (1.4-2.0)
Urine bladder	0.2 (0.1-1.4)	10.9 (10.0-33.0)	2.4 (1.8-14.9)
Tight muscle	0.0 (0-0)	1.9 (1.9-2.0)	0.5 (0.4-0.6)

Table 4. Bio-distribution of ^{68}Ga-citrate in juvenile 14-15 weeks old female domestic pigs. List of target tissues/organs encompassed by region of interest. Median values of SUV_{min}, SUV_{max}, and SUV_{mean}. Ranges in parentheses

^{68}Ga-citrate	SUV_{min}	SUV_{max}	SUV_{mean}
Brain	0.1 (0.1-0.1)	0.3 (0.3-0.4)	0.2 (0.0 -0.2)
Thymus	0.5 (0.0-0.8)	1.1 (0.0-1.2)	0.8 (0.0-0.9)
Heart	0.55 (0.2-1.5)	0.95 (0.6-8.8)	0.55 (0.5-1.2)
Lung	0.5 (0.0-0.8)	1.2 (0.0-1.6)	0.9 (0.0-1.1)
Vertebral body	0.7 (0.4-1.3)	3.0 (2.2-3.4)	2.0 (1.4-2.4)
Liver	0.6 (0.3-2.6)	1.4 (0.8-3.5)	1.0 (0.5-3.2)
Spleen	0.2 (0.0-0.3)	0.9 (0.0-1.3)	0.6 (0.0-0.7)
Gall bladder	0.2 (0.1-0.3)	0.4 (0.3-0.5)	0.3 (0.2-0.4)
Stomach	0.0 (0.0-0.0)	0.05 (0.0-0.1)	0.0 (0.0-0.0)
Small intestine	0.5 (0.0-1.4)	3.8 (0.1-4.5)	2.9 (0.0- 3.4)
Colon	0.3 (0.3-0.6)	1.3 (0.8-2.4)	0.9 (0.5-1.0)
Kidney	0.45 (0.1-0.8)	1.5 (1.5-1.5)	0.8 (0.4-1.2)
Urine bladder	0.15 (0.1-0.2)	0.4 (0.3-0.5)	0.25 (0.2-0.3)
Tight muscle	0.4 (0.1-0.1)	0.5 (0.1-0.2)	0.6 (0.1-0.0.2)

reported, S. *aureus* was isolated from the lungs in pigs 1, 2, and 4, but not from pig 3, which by clinical examination and hematology did not show any signs of infection at all [15]. The findings of S. *aureus* in the lungs corresponded to the presence of grossly visible disseminated lung abscesses in pigs 1, 2, and 4, but not pig 3, lesions that were evident also by CT (**Figure 2A**, **2B**). The lung CT scans of pigs 1 and 2 further varied in presentation from localized consolidation to diffuse infiltrative change in almost all lobes, and consecutive CT scans during the 18 h scanning protocol revealed, especially in pig 1, that lesions worsened at the late scans. Thus, non-cardiogenic edema and congestive atelectasis was prominent in this pig. Gross pathology of all pigs revealed presence of lung edema and atelectasis, changes ranging from being only focal (pig 3) to almost diffuse, and pigs 2 and 4 had pleural effusions as well. Histopathology of the lungs from pigs 1, 2 and 4 showed presence of both acute and subacute abscess-forming lesions, the latter occasionally with central necrotic lung tissue; also acute suppurating bronchopneumonia (lesions within the conductive airways and alveoli) were seen, as were aggregates of coccoid bacteria (**Figure 2C-E**). Again pig 3 was without significant lung histopathology. An acute regional suppurating tracheitis was present in pig 4, as evidenced by histopathology. Besides the respiratory system (i.e. lungs, thoracic cavity, trachea and tracheobronchial lymph nodes) three additional tissue compartments displayed changes/lesions: skeletal muscles, nasal cavities and the abdominal cavity (**Table 5**).

Foci of necrotic skeletal muscles were macroscopically evident in the dorsal neck region of all four pigs and evident as enlargement and decreased attenuation of the affected muscles

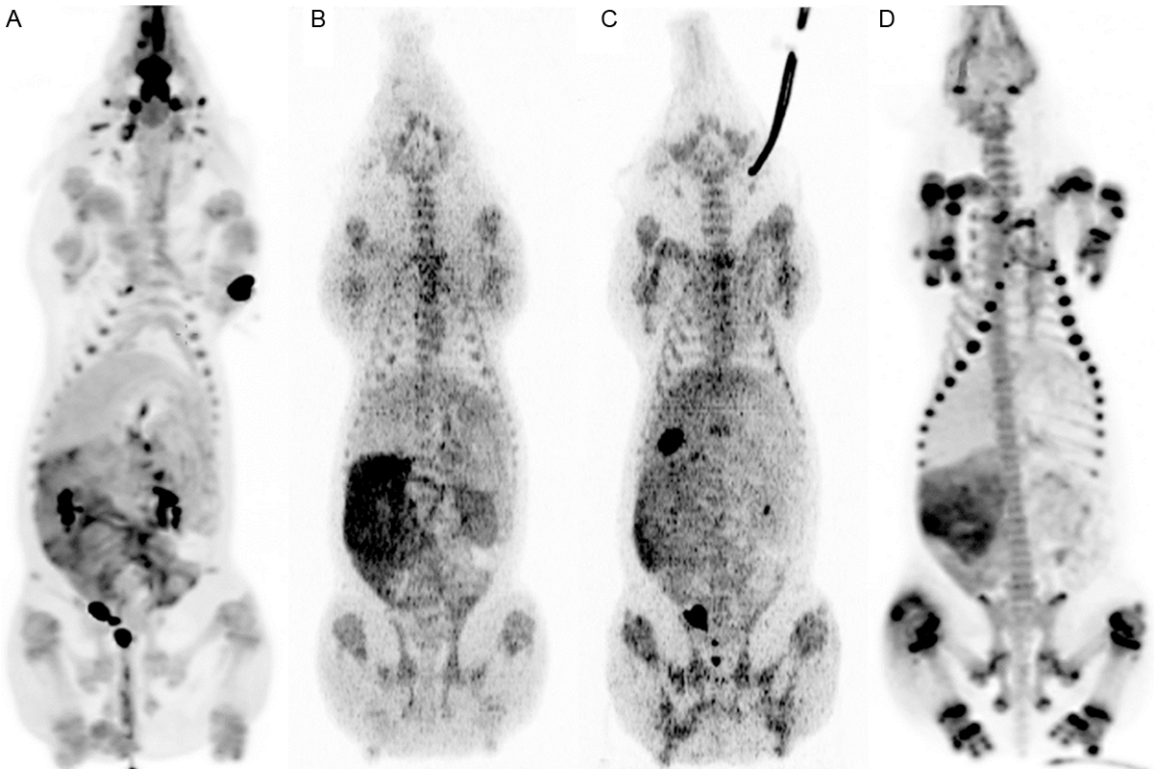

Figure 1. Maximum intensity projection (MIP) of whole bodies from ventral (anterior) view demonstrating normal distribution of various tracers in a juvenile pig without *S. aureus* infection. A: ^{18}F-FDG, B: ^{11}C-Methionine, C: ^{11}C-PK11195, and D: ^{68}Ga-citrate.

and in some cases air bubbles formations and initiation of fluid collection on CT. The necrotic lesion to the left in pig 1 had peripheral suppuration and clearly visible granulation tissue (**Figure 3A**). Histopathology was performed in pigs 1 (left lesion), 2 and 3 (right lesion) and showed the necrotic lesions to be subacute i.e. surrounded by many mononuclear cells and fibrosis although some areas were acutely affected in pig 2 as evidenced by primarily neutrophile cellular reaction. In pigs 2 and 3 a few arteries and arterioles showed evidence of vasculitis and/or thrombosis. The lesions on the left side in pig 1 additionally showed presence of intense neutrophil infiltration (suppuration) and granulation tissue formation immediately peripheral to the necrotic muscle, and presence of coccoid bacteria in clusters mainly concentrated in and around the necrotic area (**Figure 3B**, **3C**). Immunohistochemical staining of this lesion revealed the bacteria to be *S. aureus*.

Small foci of necrotic muscle were also present in the muscles dorsal to the lumbar vertebrae in pigs 2 and 3 and these foci were not evident on CT scans. Histopathology was performed on pig 2 exclusively and showed the lesions to be acute, thus dominated by neutrophils; a few arterioles had vasculitis and/or thrombosis.

Microbial cultivation of the brain, liver, spleen, kidney, and abdominal cavity (increased amount of fluid) was sterile in all four pigs except of the brain in pig 3 (moderate growth of coagulase-negative staphylococci and Gram-negative rods) and in pig 4 (few colonies of *S. aureus* and heavy growth of Escherichia coli). The additional isolates from the brains in pigs 3 and 4 were assumed to be the result of contamination during the sampling procedure.

Performance of the tracers

Table 5 aligns PET with the other recorded findings. ^{18}F-FDG, ^{11}C-PK11195, and ^{11}C-methionine all accumulated in pulmonary infectious lesions with decreasing intensity, thus ^{18}F-FDG was much superior (**Figure 4A-D**). The lymph nodes in the tracheobronchial region accumulated low amounts of ^{18}F-FDG, ^{11}C-PK11195, ^{11}C-methionine, and ^{11}C-PK11195.

Table 5. Alignment of diagnostic CT, PET (^{18}F-FDG, ^{68}Ga-citrate, ^{11}C-PK11195 and ^{11}C-methionine), gross pathology, and microbiology in head, neck, and thorax seven days after inoculation with *S. aureus* in the right femoral arteries of juvenile female domestic pigs

PIG 1	CT	PET	Gross pathology	Microbiology[A]
Skeletal muscles	Two lesions in dorsal neck muscles region, 41×35×67 and 37×28×55 mm	^{18}F-FDG ^{11}C-methionine ^{68}Ga-citrate	Two necrotic muscle foci in the dorsal neck region above vertebral body C2-4, one on each side of the midline, both 2×5×5 cm, on the left side accompanied by peripheral suppuration and granulation tissue	*S. aureus*, only left side lesion tested[C]
Lungs	Several abscess-like lung lesions, largest 17 mm in diameter	^{18}F-FDG ^{11}C-methionine ^{11}C-PK11195	Disseminated lung abscesses	*S. aureus* (heavy growth)
	Partly consolidated, infiltrative and atelectatic changes in dorsocaudal part of left lung, 59×47×44 mm and pleura effusions; atelectatic changes in right lung	^{18}F-FDG ^{11}C-methionine ^{11}C-PK11195	Bilateral diffuse atelectasis and edema	NT[D]
Tracheobronchial lymph nodes[E]	11 mm (short axis) left side	^{18}F-FDG	NT	NT
Nasal cavities	Discrete mucous membrane swelling	^{18}F-FDG	NT	NT
Abdominal cavity	—[B]	—	Increased amount of abdominal fluid with some fibrin flakes	Sterile
PIG 2	**CT**	**PET**	**Gross pathology**	**Microbiology[A]**
Skeletal muscles	Three contiguous ring-shaped lesions in the dorsal neck muscle region, largest 34×21×49 mm	^{18}F-FDG	One 1×4×4 cm rounded necrotic muscle focus in the dorsal neck region	NT
	Hardly visible	^{18}F-FDG (very discrete)	One 1×2×2 cm necrotic muscle focus in the region dorsal to the lumbar vertebrae	NT
Lungs	Multiple lung abscesses, largest 16 mm in diameter	^{18}F-FDG	Disseminated lung abscesses, largest 1 cm in diameter, some had elicited acute focal fibrinous pleuritis; several pinpoint lesions	*S. aureus* (heavy growth)
	Diffuse consolidated and infiltrative changes in dorsocaudal lung areas, especially the left lung	^{18}F-FDG	Bilateral diffuse atelectasis and edema	NT
	—	—	Increased amount of clear fluid in pleural cavity	*S. aureus* (heavy growth)
Tracheobronchial lymph nodes[E]	12 mm (short axis) right and left side; 11 mm (short axis) left lung hilus	^{18}F-FDG ^{11}C-methionine ^{11}C-PK11195	NT	NT
Nasal cavities	Discrete mucous membrane swelling	^{18}F-FDG	NT	NT
Abdominal cavity	Light ascites on late scans	—	Increased amount of abdominal fluid with some fibrin flakes	Sterile
PIG 3	**CT**	**PET**	**Gross pathology**	**Microbiology**
Skeletal muscles	Two contiguous “8”-shaped lesions with air formation in the dorsal neck muscle region, 51×26×21 mm and 50×27×21 mm.	^{18}F-FDG ^{11}C-PK11195 (in subcutaneous fat tissue above the abscess)	Two, 1×3×4 cm and 1×2×2 cm, necrotic muscle foci in the dorsal neck region on the left side; one 1×3×5 cm necrotic muscle focus in the dorsal neck region on the right side	*P. multocida* (few colonies)[F], only right side lesion tested
	—	Discrete ^{18}F-FDG	One necrosis-like muscle focus in the region dorsal to the lumbar vertebrae	NT
Lungs	Infiltrative diffuse dorsocaudal changes[G]	—	Bilateral and dorsocaudal located areas of atelectasis (5×5×5 cm); moderate bilateral edema; disseminated acute petechial	Sterile

Tracheobronchial lymph nodes[E]	8 mm (short axis) right side	^{18}F-FDG	NT	NT
		^{11}C-methionine		
		^{11}C-PK11195		
Nasal cavities	Discrete mucous membrane swelling bilat	^{18}F-FDG	NT	NT
Abdominal cavity	---	---	Increased amount of abdominal fluid with some fibrin flakes	Sterile
PIG 4	CT	PET	Gross pathology	Microbiology[A]
Skeletal muscles	Two lesions in the dorsal neck muscle region on the right side, 29×18×8 mm and 28×19×9 mm; a small discrete abscess-like lesion on the left side	^{18}F-FDG	Two necrotic muscle foci in the dorsal neck region on the right side, largest 2×5×5 mm	NT
		^{11}C-PK11195 (in subcutaneous fat tissue above the abscess)		
Lungs	Multiple lung abscesses, largest 24 mm in diameter	^{18}F-FDG	Disseminated lung abscesses, largest 2 cm in diameter	*S. aureus* (heavy growth)
		^{11}C-methionine		
		^{11}C-PK11195		
	---[H]	---	Bilateral dorsocaudal atelectasis; moderate bilateral diffuse edema	*E. coli* (heavy growth)[F]; coagulase-negative staphylococci (moderate growth)[F]
	---[I]	---	100 ml of sanguineous pleural fluid, both right and left thoracic cavities	*E. coli* (heavy growth)[F]
	---	---	Edema an hyperemia of the tracheal mucosa distal to the larynx	NT
Tracheobronchial lymph nodes[E]	8 mm (short axis) right side	^{11}C-methionine	NT	NT
		^{11}C-PK11195 (weak)		
Nasal cavities	Discrete mucous membrane swelling	^{18}F-FDG	NT	NT
Abdominal cavity	Minimal ascites on last scan	---	Increased amount of abdominal fluid with some fibrin flakes	Sterile

[A]: All *S. aureus* isolates form the pigs were phenotypically indistinguishable from the inoculated strain, [B]: --- indicates absence of signal within the stated tissue compartment, [C]: The lesion was tested for presence of *S. aureus* by immunohistochemistry, [D]: NT indicates not tested, [E]: The precise correspondence of the affected tracheobronchial lymph nodes (four groups) was difficult to establish, [F]: The microbial results were believed to represent contamination, [G]: No atelectasis or edemas on last scan, [H]: No atelectasis on last scan, and [I]: No pleural effusions on last scan.

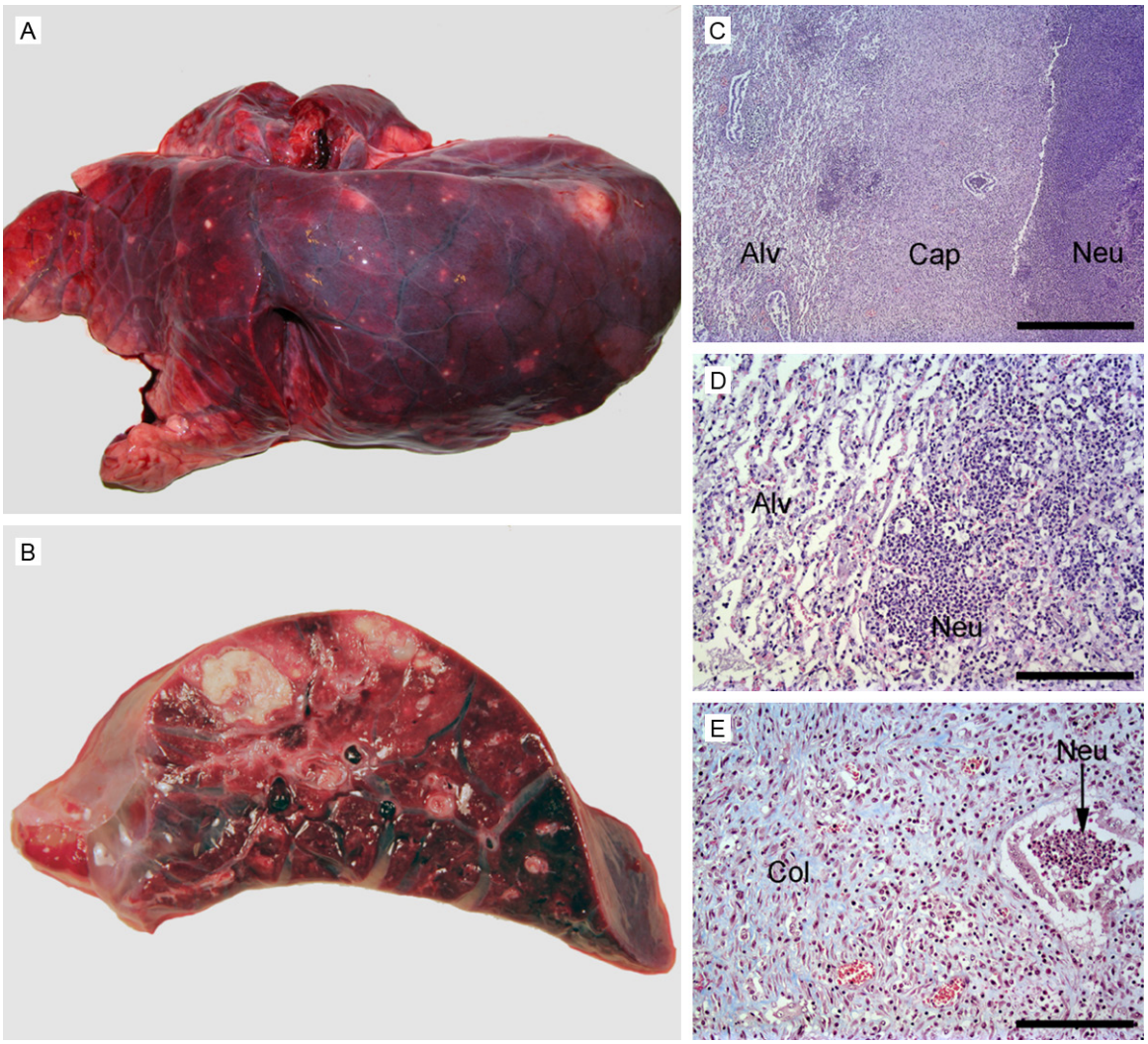

Figure 2. Gross pathology of abscesses in the lungs (A, B). (A) Costal surface of left lung, pig 2, with disseminated abscesses. (B) Transverse section, pig 1, presenting two abscesses. (C-E) Histopathology of the capsule of a subacute lung abscess, pig 4 (C-E). (C) Haematoxylin and eosin staining displayed neutrophils (Neu), a capsule (Cap) consisting of granulation tissue, and surrounding atelectatic lung alveoli (Alv). Bar = 1 mm. (D) Haematoxylin and eosin staining of lung tissue peripheral to the abscess capsule, demonstrating acute suppuration, i.e. presence of neutrophils (Neu), into the alveoli, and atelectatic alveoli (Alv). (E) Masson trichrome staining (collagen is stained blue) of the central part of the abscess capsule, showing abundance of collagen (Col) and neutrophils (Neu) within a bronchiole. Bar (D, E) = 100 μm.

The necrotic infected suppurating lesions in the dorsal neck muscles accumulated ^{18}F-FDG in all pigs and accumulation of ^{11}C-methionine and ^{68}Ga-citrate was much lower (**Figure 5A-C**). Low ^{18}F-FDG activity was also registered in the acute or inflamed lesions in the neck muscles and only slight ^{18}F-FDG activity was seen in the margin of the muscular lesions in the lumbar region, none of the other tracers accumulated in these areas except for ^{11}C-PK11195 that showed slight accumulation in the subcutaneous edematous tissue overlaying these lesions.

Table 6 presents the number of gross pathology and/or CT lesions identified by the individual tracers. The number and size in the initial scans of lung lesions were more or less well defined in pigs 1, 2, and 4, but at the end of the 18 h scanning protocols they were more confluent. ^{18}F-FDG was in general better than the other tracers at detecting most lesions, especially pulmonary lesions and neck lesions, whereas the other tracers being almost equally *non*-accumulating and just accumulating in reactive lymph nodes of the tracheobronchial region.

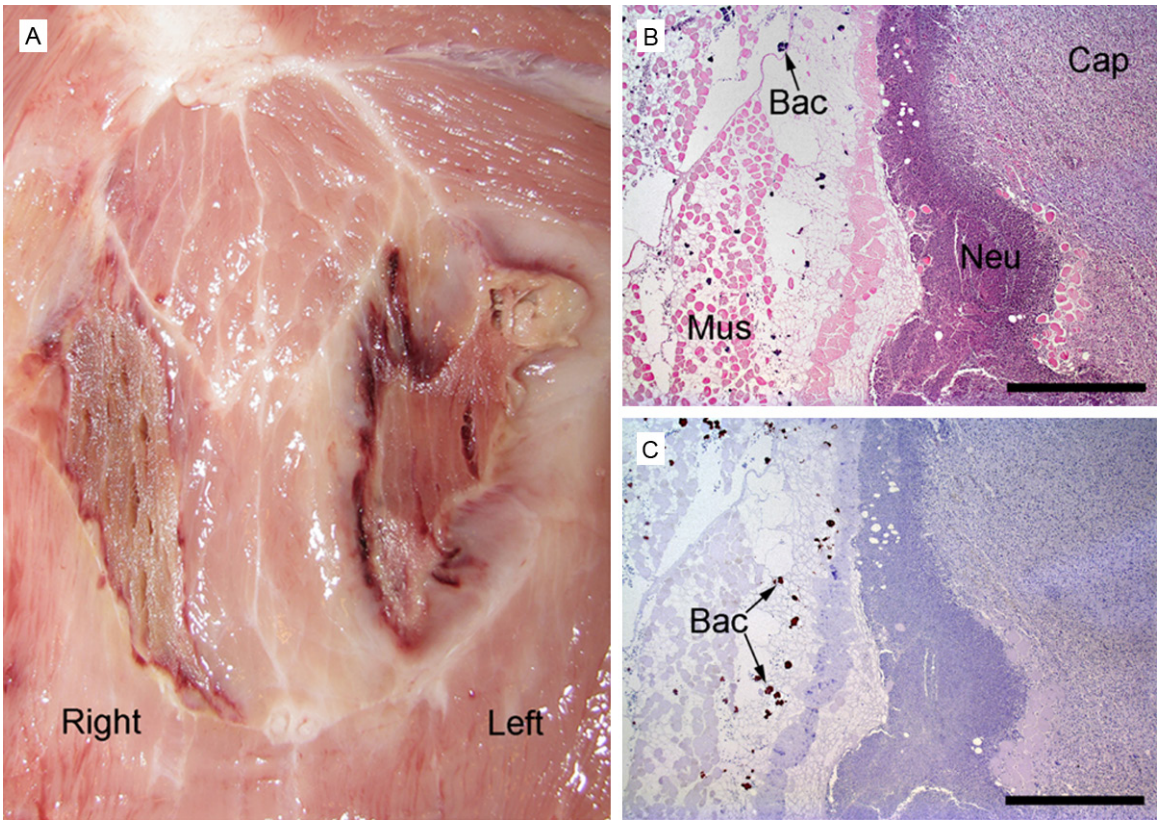

Figure 3. Gross pathology of skeletal muscle necroses in the neck region, pig 1 (A). The lesion in the left muscle has peripheral suppuration. Histopathology of skeletal muscle lesion consisting of necrosis and peripheral suppuration (left-sided lesion in A), (B, C) pig 1. Haematoxylin and eosin stain demonstrates capsule formation (Cap) consisting of granulation tissue, neutrophils (Neu), and necrotic transversely sectioned striated muscle cells (Mus) and bacterial colonies (Bac) (B). Same region stained immunohistocytochemically identifying *S. aureus* bacteria (Bac) (C). Bar (B, C) = 1 mm.

Discussion

Bio-distribution of the PET tracers ^{18}F-FDG, ^{11}C-PK11195, ^{11}C-methionine, and ^{68}Ga-citrate in juvenile pigs is presented and the bio-distribution differs slightly from that in humans [28]. PET/CT diagnostics produce high-spatial-resolution functional tomographic images that are then fused to low-dose anatomic CT images, exactly localizing all the pathologic findings. ^{18}F-FDG and ^{68}Ga-citrate in this context demonstrated the best imaging quality with higher infection/inflammation to background ratio making interpretation of PET better than with ^{11}C-PK11195 and ^{11}C-methionine, both of which had substantial background uptake.

Hoffer [28] reported high concentrations of lactoferrin in neutrophils and in abscess fluids and suggested that ^{67}Ga-citrate binding to lactoferrin is a major factor in the mechanism of accumulation of ^{67}Ga-citrate in abscesses. On the other hand, ^{18}F-FDG uptake in infectious lesions has been considered due to inflammatory cells (i.e., leukocytes and macrophages) [40-42] and granulation tissue [42, 43]. Activated leukocytes and macrophages in inflammatory tissue utilize glucose as an energy source for chemotaxis and phagocytosis [44] and can increase both oxygen consumption and glucose metabolism in response to infection via the hexose monophosphate shunt, depending on the cell and the nature of the stimulus [40]. In addition, increased vascular permeability and increased blood flow due to newly formed or dilated blood vessels may cause some increase in local tracer uptake [45, 46].

In the current animal model necrotic muscle areas, with or without pronounced secondary peripheral suppuration, were present in the neck (big lesions) and sacral muscles (small

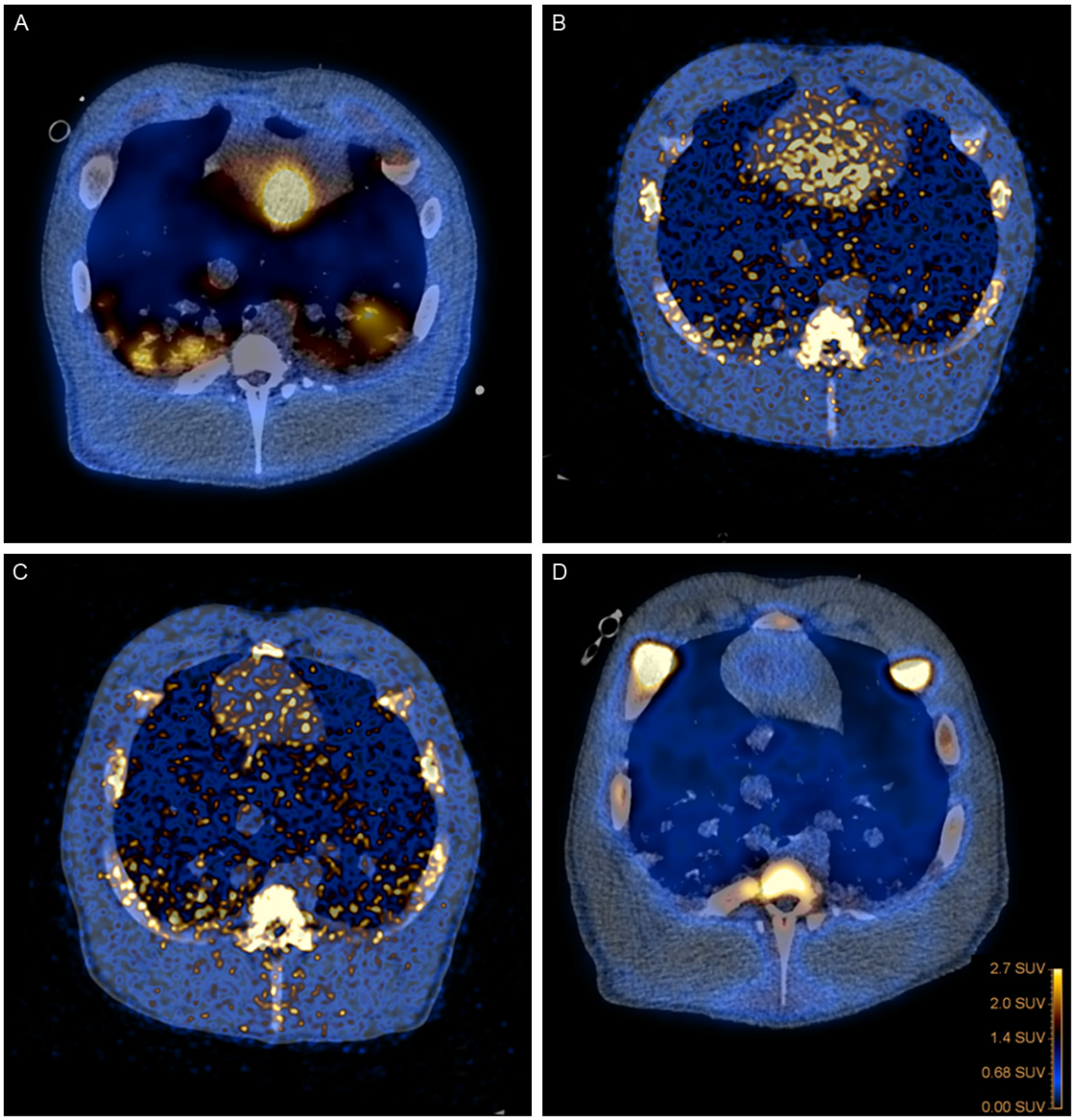

Figure 4. Fused PET/CT images of lungs with abscesses and axial views, with A: ^{18}F-FDG, B: ^{11}C-Methionine, C: ^{11}C-PK11195, and D: ^{68}Ga-citrate.

lesions). The lesions in the neck muscles may have been formed as a consequence of repeated intramuscular injections of e.g. painkillers, and at least one of these lesions seems to have become secondarily infected with *S. aureus*. Especially this type of lesion showed higher tracer-uptake in the margin than in the surrounding edematous muscle and in the center. It has been reported that abscess-forming bacteria utilize glucose as an energy source through various pathways [47]. The apparent lack of ^{18}F-FDG uptake in the necrotic muscle centers could be attributed to low numbers of inflammatory cells since changing the color scale reading the PET scans did demonstrate very low FDG-uptake in the margins of the lesions probably due to presence of granulation tissue. Most areas were examined microscopically and categorized by its predominant histological characteristic as either necrosis, inflammatory or infectious (**Table 5**). ^{11}C-Methionine and ^{68}Ga-citrate also demonstrated uptake in the suppurating lesions, but ^{11}C-PK11195 did not. ^{18}F-FDG was able to help detecting necrotic lesions in muscles difficult to distinguish on CT scans, especially in very

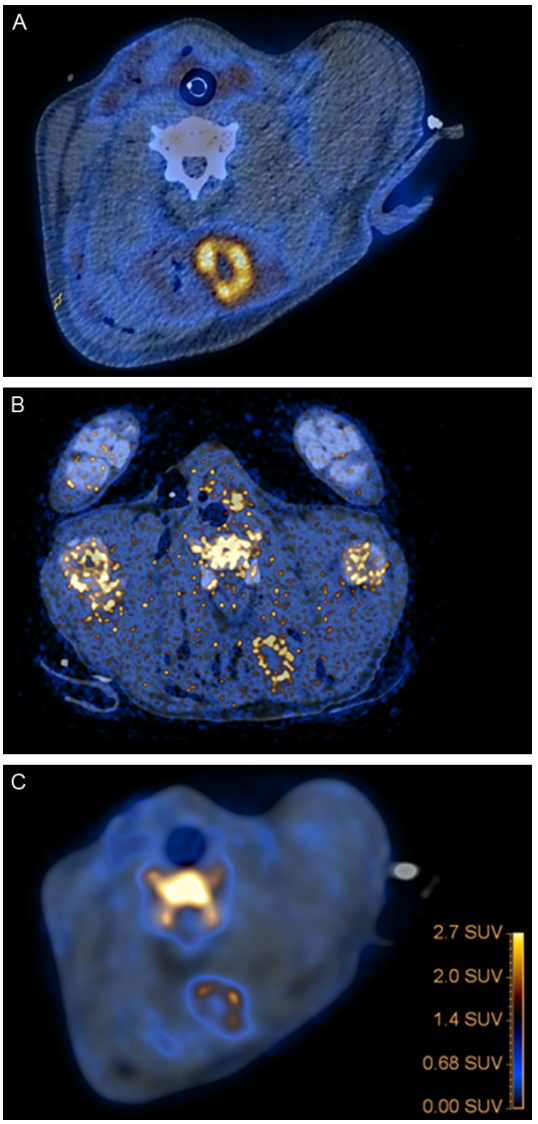

Figure 5. Fused PET/CT images, axial views, with ^{18}F-FDG (A), ^{11}C-Methionine (B), and ^{68}Ga-citrate (C). (A and C) has been aligned to (B) so that the cervical vertebra all are in the same plane. Neck region with muscle necroses. The left muscle had *S. aureus* infection and peripheral suppuration. High tracer-uptake in lesion of the left muscle and only faint uptake of solely ^{18}F-FDG in the margin of the necrotic areas in the right muscle.

small lesions where changing the color scale was very helpful.

^{18}F-FDG was much superior to the other tracers in detecting pulmonary abscesses and infiltrative changes. Overall, it was a bit surprising that, in our hands, almost no detection of infectious foci was seen with ^{68}Ga-Citrate but the mechanism of ^{68}Ga-citrate uptake in infections is complex and not yet fully elucidated and the radiopharmaceutical has been prepared in a slightly different manner [36] than in other studies, which we believe is not sufficient to explain this unexpected finding. It is also unlikely that the protocol had any effect on the biodistribution of gallium-68. Citrate simply acts as a loosely bound counter ion, when ^{68}Ga-Citrate is injected into the bloodstream and taken up by transferrin. At the infection site it is known that bacteria produce and use siderophores to accommodate their need for iron. Iron and gallium is similar in size and charge so siderophores will not discriminate iron from gallium. Other parameters which play part in the accumulation and retention of iron and/or gallium are the presence of lactoferrin in high concentration, pH, and increased cellular permeability.

We saw no retention of blood-borne *S. aureus* in liver or spleen. Bacteremia was induced by injection of *S. aureus* the viability of which was confirmed within 24 h and kept at 4°C until transported to the animal facility. We observed no physiological response to the injection, and the pigs had a normal behavior when they had recovered from anesthesia. The blood neutrophil count and plasma C-reactive protein were monitored during development of the model demonstrating only a modest response to the inoculation [15] and this may be ascribed to the immunological age (14-15 weeks) of the pigs [48, 49]. It is well established that that the lungs in pigs play a crucial role in clearance of bacteria from the bloodstream [50], a capacity which resides in the spleen and liver in humans [51, 52] and the effector cells most probably are pulmonary intravascular macrophages. Studies have assessed aspects of immunocellular development and immunoglobulin maturity in pigs and found that immunity develops at 5 to 7 weeks of age and are fully developed at 7 to 12 week of age. The clearance capacity of bacteria in the lungs may have been exceeded, but may have been sufficient in pig 3 avoiding bacteria to settle in bones [15] and lungs.

The pulmonary lesions progressed during late scans especially in pig 1, and some of the lesions may be ascribed to the long anesthesia and recumbent positioned period, or to progression of the untreated infection and thus the bacteremia or the hematogenously dissem-

Table 6. Number of gross pathology and/or CT lesions identified by the individual tracers

Lesion	Number	Tracers			
		^{18}F-FDG	^{68}Ga-citrate	^{11}C-methionine	^{11}C-PK11195
Necroses in muscles	12	12	1	1	0
Lung abscess	NT[A]	+++	(+)	(+)	(+)
Tracheobronchial lymph nodes	6	5	0	5	5

NT: Not tested. [A]: At the initial scans of lung lesions these were more or less well defined, but at the end of the 18 h long scan protocol (the ^{18}F-FDG scan) the lesions became more diffuse; thus the number of abscesses in the lungs cannot be counted.

inated lung lesion *per se* and the pulmonary dysfunction during bacteremia may be causal or a coincidental association. The pattern of pulmonary lesions we saw in the pigs including *non*-cardiogenic edema, and congestive atelectasis was much similar to sepsis induced acute respiratory distress syndrome (ARDS) in humans [53]. In a recent study of hematogenously disseminated lung abscesses in pigs inoculated intravenous with the same porcine *S. aureus* strain as we used here, the most severe lung lesions were seen to spread to alveoli of the conducting system [54]. The type of spread was also observed in the present study, and this probably is the reason why the lungs by CT attained diffuse infiltrative changes mimicking ARDS.

Conclusions

Early identification and localization of infection is critical for the appropriate and timely selection of therapy and conventional X-ray, CT, MRI, and ultrasound are often first-line imaging methods for identification and localization of infection. These methods are, however, not always successful in finding the site of infection, particularly in patients without localizing signs or symptoms and if there are no focal fluid collection or other morphological changes. PET may improve infection diagnostics in combination with CT and in this study we found ^{18}F-FDG PET/CT to be a good supplemental to other imaging procedures for detection of infectious foci. This tracer had higher infection to background ratios and it accumulated in most infectious foci caused by *S. aureus* in juvenile female pigs, while ^{11}C-methionine and particularly ^{11}C-PK11195 and ^{68}Ga-citrate accumulated to a lesser extent in such foci.

^{18}F-FDG localized in areas with presence of inflammatory cells and bacteria, and to a lesser extent in reparative infiltration tissue surrounding necrotic lesions.

It was possible to keep the pigs anesthetized and alive during the extensive examination period despite severe progression of the untreated pulmonary infections.

Acknowledgements

This work was supported by grant no. 0602-01911B (11-107077) from the Danish Council for Independent Research, Technology and Production Sciences. The authors are grateful for the technical support provided by Dennis Brok, Malene Hylle, Hanne Thaagaard Larsen, Rikke Skall, Janne Frederiksen, Lotte S. Meyer, Lena Mortensen, Helle Danielsen, Dorte Smith, Rikke Bertelsen, Karin M Nielsen, and Dirk Bender.

Disclosure of conflicts of interest

None.

Address correspondence to: Dr. Pia Afzelius, Department of Diagnostic Imaging, North Zealand Hospital, Hillerød, Denmark. E-mail: pia.afzelius@dadlnet.dk

References

[1] Laupland KB, Lyytikäinen O, Søgaard M, Kennedy KJ, Knudsen JD, Ostergaard C, Galbraith JC, Valiquette L, Jacobsson G, Collignon P, Schønheyder HC; International Bacteremia Surveillance Collaborative. The changing epidemiology of Staphylococcus aureus bloodstream infection: a multinational population-based surveillance study. Clin Microbiol Infect 2013; 19: 465-71.

[2] Tom S, Galbraith JC, Valiquette L, Jacobsson G, Collignon P, Schønheyder HC, Søgaard M, Kennedy KJ, Knudsen JD, Ostergaard C, Lyytikäinen O, Laupland KB; International Bacteraemia Surveillance Collaborative. Case fatality ratio and mortality rate trends of community-onset Staphylococcus aureus bacteraemia. Clin Microbiol Infect 2014; 20: 630-2.

[3] Fowler VG Jr, Sanders LL, Sexton DJ, Kong L, Marr KA, Gopal AK, Gottlieb G, McClelland RS, Corey GR. Outcome of Staphylococcus aureus bacteremia according to compliance with recommendations of infectious diseases specialists: experience with 244 patients. Clinic Infect Dis 1998; 27: 478-486.

[4] Liu C, Bayer A, Cosgrove SE, Daum RS, Fridkin SK, Gorwitz RJ, Kaplan SL, Karchmer AW, Levine DP, Murray BE, J Rybak M, Talan DA, Chambers HF; Infectious Diseases Society of America. Clinical practice guidelines by the Infectious Diseases Society of America for the treatment of methicillin-resistant Staphylococcus aureus infections in adults and children. Clin Infect Dis 2011; 52: e18-55. Erratum in: Clin Infect Dis 2011; 53: 319.

[5] Steinmetz T, Eliakim-Raz N, Goldberg E, Leibovici, Yahav D. Association of vancomycin serum concentrations with efficacy in patients with MRSA infections: a systematic review and meta-analysis. Clin Microbiol Infect 2015: 21; 665-673.

[6] McAfee JG and Thaku ML. Survey of radioactive agents for in vitro labelling of phagocytic leukocytes I. Soluble agents. J Nucl Med 1976a: 17; 480-487.

[7] McAfee JG and Thaku ML. Survey of radioactive agents for in vitro labelling of phagocytic leukocytes II. Soluble agents. J Nucl Med 1976: 17; 488-490.

[8] El-Maghraby TA, Moustafa HM and Pauwels EK. Nuclear medicine methods for evaluation of skeletal infection among other diagnostic modalities. Q J Nucl Med Mol Imaging 2006; 50: 167-192.

[9] Deysine M, Robinson R, Rafkin H, Teicher I, Silver L and Aufses AH. Clinical Infections Detected by ^{67}Ga Scanning. Ann Surg 1974: 897-901.

[10] Balair DC, Carroll M, Carr EA, Fekety FR. 67Ga-Citrate for Scanning Experimental Staphylococcal Abscesses. J Nucl Med 1973: 14; 99-102.

[11] Burleson RL, Johnson MC and Head H. Scintigraphic Demonstration of Experimental Abscesses with Intravenous ^{67}Ga Citrate and ^{67}Ga Labeled Blood Leukocytes. Ann Surg 1973; 178: 446-451.

[12] Gelrud LG, Arseneau JC and Johnston GS. Gallium-67 Localization In Experimental and Clinical Abscesses (Abstr). Clin Res 1972; 20: 881.

[13] Littenberg RL, Taketa RM, Alazraki NP, Halpern SE and Ashburn WL. Gallium-67 for Localization of Septic Lesions. Ann Intern Med 1973; 79: 403-406.

[14] Gravius S, Gebhard M, Ackermann D, Büll U, Hermanns-Sachweh B and Mumme T. Analysis af ^{18}F-FDG uptake pattern in PET for aseptic loosening versus prosthesis infection after total knee artoplasty: a prospective pilot study. Nuklearmedizin 2010; 49: 115-123.

[15] Nielsen OL, Afzelius P, Bender D, Schønheyder HC, Leifsson P, Nielsen K, Larsen J, Jensen SB and Alstrup AK. Comparison of autologous ^{111}In-leukocytes, ^{18}F-FDG, ^{11}C-methionine, ^{11}C-PK11195, ^{68}Ga-citrate for diagnostic nuclear imaging in a juvenile porcine haematogenous *staphylococcus aureus* osteomyelitis model. Am J Nucl Med Mol Imaging 2015; 5: 169-182.

[16] Johansen LK and Jensen HE. Animal models of hematogenous *Staphylococcus aureus* osteomyelitis in long bones: a review. Orthop Res Rev 2013; 5: 51-64.

[17] Hirata K, Shiga T, Fujima N, Manabe O, Usui R, Kuge Y and Tamaki N. 11C-Methionine positron emission tomography may monitor the activity of encephalitis. Acta Radiol 2012; 53: 1155-1157.

[18] Zhao S, Kuge Y, Kohanawa M, Takahashi T, Zhao Y, Yi M, Kanegae K, Seki K and Tamaki N. Usefulness of 11C-methionine for differentiating tumors from granulomas in experimental rat models: a comparison with 18F-FDG and 18F-FLT. J Nucl Med 2008; 49: 135-141.

[19] Banati RB, Newcombe J, Gunn RN, Cagnin A, Turkheimer F, Heppner F, Price G, Wegner F, Giovannoni G, Miller DH, Perkin GD, Smith T, Hewson AK, Bydder G, Kreutzberg GW, Jones T, Cuzner ML and Myers R. The peripheralbenzodiazepine binding site in the brain in multiple sclerosis: quantitative *in vivo* imaging of microglia as a measure of disease activity. Brain 2000; 123: 2321-2337.

[20] Turner MR, Cagnin A, Turkheimer FE, Miller CC, Shaw CE, Brooks DJ, Leigh PN and Banati RB. Evidence of widespread cerebral microglial activation in amyotrophic lateral sclerosis: an [11C](R)-PK11195 positron emission tomography study. Neurobiol Dis 2004; 15: 601-9.

[21] Cagnin A, Gerhard A and Banati RB. In vivo imaging of neuroinflammation. Eur Neuropsychopharm 2002; 12: 581-586.

[22] Ren W, Muzik O, Jackson N, Khoury B, Shi T, Flynn JC, Chakraborty P and Markel DC. Differentiation of septic and aseptic loosening by PET with both 11C-PK11195 and 18F-FDG in rat models. Nucl Med Commun 2012; 33: 747-756.

[23] Pugliese F, Gaemperli O, Kinderlerer AR, Lamare F, Shalhoub J, Davies AH, Rimoldi OE, Mason JC and Camici PG. Imaging of Vascular Inflammation With [11C]-PK11195 and Positron Emission Tomography/Computed Tomo= graphy Angiography. J Amer Coll Cardiol 2010; 56: 653-661.

[24] Roivainen A, Någren K, Hirvonen J, Oikonen V, Virsu P and Tolvanen T. Whole-body distribution and metabolism of [N-methyl-11C](R)-1-(2-chlorophenyl)-N-(1-methylpropyl)-3-isoquinoline carboxamide in man: an imaging agent for *in vivo* assessment of peripheral benzodiazepine receptor activity with positron emission

tomography. Eur J Nucl Med Mol Imaging 2009; 36: 671-82.
[25] Hirvonen J, Roivainen A, Virta J, Helin S, Någren K and Rinne JO. Human biodistribution and radiation dosimetry of 11C-(R)-PK11195: the prototypic PET ligand to image inflammation. Eur J Nucl Med Mol Imaging 2010; 37: 606-12.
[26] Kumar A, Muzik O, Chugani D, Chakraborty P and Chugani HT. PETderived biodistribution and dosimetry of the benzodiazepine receptor-binding radioligand (11)C-(R)-PK11195 in children and adults. J Nucl Med 2010; 51: 139-44.
[27] Nanni C, Errani C, Boriani L, Fantini L, Ambrosini V, Boschi S, Rubello D, Pettinato C, Mercuri M, Gasbarrini A and Fanti S. 68Ga-citrate PET/CT for evaluating patients with infections of the bone: preliminary results. J Nucl Med 2010; 51: 1932-1936.
[28] Hoffer P. Gallium: mechanisms. J Nucl Med 1980; 21: 282-285.
[29] Palestro CJ, Brown ML, Greenspan BS, McAfee JG, Royal HD, Schauwecker DS, Seabold JE and Signore A. Society of Nuclear Medicine Procedure Guideline for Gallium Scintigraphy in Inflammation Version 3.0. approved June 2, Rome University La Sapienza 2004. pp. 1-5.
[30] Kumar V, Boddeti DK, Evans SG and Angelides S. (68)Ga-Citrate-PET for diagnostic imaging of infection in rats and for intra-abdominal infection in a patient. Curr Radiopharm 2012; 5: 71-75.
[31] Leifsson PS, Iburg T, Jensen HE, Agerholm JS, Kjelgaard-Hansen M, Wiinberg B, Heegaard PM, Astrup LB, Olsson AE, Skov MG, Aalbaek B and Nielsen OL. Intravenous inoculation of Staphylococcus aureus in pigs induces severe sepsis as indicated by increased hypercoagulability and hepatic dysfunction. FEMS Microbiol Lett 2010; 309: 208-216.
[32] Hasman H, Moodley A, Guardabassi L, Stegger M, Skov RL and Aarestrup FM. Spa type distribution in Staphylococcus aureus originating from pigs, cattle and poultry. Vet Microbiol 2010; 141: 326-331.
[33] Nielsen OL, Iburg T, Aalbaek B, Leifsson PS, Agerholm JS, Heegaard P, Boye M, Simon S, Jensen KB, Christensen S, Melsen K, Bak AK, Backman ER, Jorgensen MH, Groegler DK, Jensen AL, Kjelgaard-Hansen M and Jensen HE. A pig model of acute Staphylococcus aureus induced pyemia. Acta Vet Scand 2009; 51: 14-21.
[34] Comar D, Cartron J, Maziere M and Marazano C. Labelling and metabolism of methionine-methyl-11 C. Eur J Nucl Med 1976; 1: 11-14.
[35] Shah F, Hume SP, Pike VW, Ashworth S and McDermott J. Synthesis of the enantiomers of [N-methyl-11C]PK 11195 and comparison of their behaviours as radioligands for PK binding sites in rats. Nucl Med Biol 1994; 21: 573-581.
[36] Jensen SB, Nielsen KM, Mewis D and Kaufmann J. Fast and simple one-step preparation of (6)(8)Ga citrate for routine clinical PET. Nucl Med Commun 2013; 34: 806-812.
[37] Alstrup AK and Winterdahl M. Imaging Techniques in Large Animals. Scand J Lab Anim Sci 2009; 36: 55-66.
[38] Madsen LW and Jensen HE. Necropsy of the Pig. In: Jensen HE, editor. Necropsy A Handbook and Atlas. Frederiksberg: Biofolia; 2011; pp. 83-106.
[39] Jensen HE, Nielsen OL, Agerholm JS, Iburg T, Johansen LK, Johannesson E, Møller M, Jahn L, Munk L, Aalbaek B and Leifsson PS. A non-traumatic Staphylococcus aureus osteomyelitis model in pigs. In Vivo 2010; 24: 257-264.
[40] Fantone JC and Ward PA. Role of oxygen-derived free radicals and metabolites in leukocyte-dependent inflammatory reactions. Am J Pathol 1982; 107: 395-418.
[41] Osman S and Danpure HJ. The use of 2-[18F] fluoro-2-deoxy-Dglucose as a potential in vitro agent for labelling human granulocytes for clinical studies by positron emission tomography. Int J Rad Appl Instrum B 1992; 19: 183-190.
[42] Kubota R, Yamada S, Kubota K, Ishiwata K, Tamahashi N and Ido T. Intratumoral distribution of fluorine-18-fluorodeoxyglucose in vivo: high accumulation in macrophages and granulation tissues studied by microautoradiography. J Nucl Med 1992; 33: 1972-1980.
[43] Yamada S, Kubota K, Kubota R, Ido T and Tamahashi N. High accumulation of fluorine-18-fluorodeoxyglucose in turpentine-induced inflammatory tissue. J Nucl Med 1995; 36: 1301-1306.
[44] Weisdorf DJ, Craddock PR and Jacob HS. Glycogenolysis versus glucose transport in human granulocytes: differential activation in phagocytosis and chemotaxis. Blood 1982; 60: 888-893.
[45] Minn H, Paul R and Ahonen A. Evaluation of treatment response to radiotherapy in head and neck cancer with fluorine-18 fluorodeoxyglucose. J Nucl Med 1988; 29: 1521-1525.
[46] Ichiya Y, Kuwabara Y, Sasaki M, Yoshida T, Akashi Y, Murayama S, Nakamura K, Fukumura T and Masuka K. FDG-PET in infectious lesions: the detection and assessment of lesion activity. Ann Nucl Med 1996; 10: 185-191.
[47] Anderson RL and Wood WA. Carbohydrate metabolism in microorganisms. Ann Rev Microbiol 1969; 23: 539-578.

[48] Juul-Madsen HR, Jensen KH, Nielsen J and Damgaard BM. Ontogeny and characterization of blood leukocyte subsets and serum proteins in piglets before and after weaning. Vet Immunol Immunopath 2010; 133: 95-108.
[49] Alstrup AK, Nielsen KM, Schønheyder HC, Jensen SB, Afzelius P, Leifsson PS and Nielsen OL. Refinement of a hematogenous localized osteomyelitis model in pigs. Submittet to SJLAS 2015.
[50] Ricci MA, Mehran R, Christou NV, Mohamed F, Graham AM and Symes JF. Species differences in the clearance of Staphylococcus aureus bacteremia. J Invest Surg 1991; 4: 53-8.
[51] Beeson PB, Brannon ES and Warren JV. Observations on the sites of removal of bacteria from the blood in patients with bacterial endocarditis. J Exp Med 1945; 81: 9-23.
[52] Bennett IL Jr, Beeson PB. Bacteremia: a consideration of some experimental and clinical aspects. Yale J Biol Med 1954; 26: 241-62.
[53] Ashbaygh DG, Bigelow DB, Petty TK and Levine BE. Acute respiratory distress in adults. Lancet 1967; 290; 319-323.
[54] Soerensen KE, Skovgaard K, Heegaard PM, Jensen HE, Nielsen OL, Leifsson PS, Olsen HG, Aalbaek B, Kristensen AT, Kjeldgaard-Hansen M, Wiinberg B and Iburg TM. The imapct of Staphylococcus aureus concentration on the development of pulmonary lesions and cytokine expression after intravenous inoculation of pigs. J Vet Pathol 2012; 49: 950-962.